atoms

MDPI

Article

Radiative and Collisional Molecular Data and Virtual Laboratory Astrophysics

Vladimir A. Srećković [1,*], Ljubinko M. Ignjatović [1], Darko Jevremović [2], Veljko Vujčić [2,3] and Milan S. Dimitrijević [2,4]

1 Institute of Physics, Belgrade University, Pregrevica 118, Zemun, 11080 Belgrade, Serbia; ljuba@ipb.ac.rs
2 Astronomical Observatory, Volgina 7, 11060 Belgrade, Serbia; darko@aob.rs (D.J.); veljko@aob.rs (V.V.); mdimitrijevic@aob.rs (M.S.D.)
3 Faculty of Organizational Sciences, University of Belgrade, Jove Ilica 154, 11000 Belgrade, Serbia
4 LERMA, Observatoire de Paris, UMR CNRS 8112, UPMC, 92195 Meudon CEDEX, France
* Correspondence: vlada@ipb.ac.rs; Tel.: +381-(0)-11-37-13-000

Academic Editor: Elmar Träbert
Received: 4 September 2017; Accepted: 13 September 2017; Published: 19 September 2017

Abstract: Spectroscopy has been crucial for our understanding of physical and chemical phenomena. The interpretation of interstellar line spectra with radiative transfer calculations usually requires two kinds of molecular input data: spectroscopic data (such as energy levels, statistical weights, transition probabilities, etc.) and collision data. This contribution describes how such data are collected, stored, and which limitations exist. Also, here we summarize challenges of atomic/molecular databases and point out our experiences, problems, etc., which we are faced with. We present overview of future developments and needs in the areas of radiative transfer and molecular data.

Keywords: atomic/molecular data; radiative and collisional processes; stars

1. Introduction

Many fields in astronomy such as astrophysics, astrochemistry and astrobiology, depend on data for atomic and molecular (A + M) collision and radiative processes. Among these amount of data collections there are atomic and molecular processes and spectral regions that even today are poorly represented. Therefore, there is an urgent need to collect these data in the databases as well as to develop methods for improving the existing ones. Also, this require a joint effort both of scientists and IT software specialists to develop state-of-the-art infrastructures satisfying their needs, such as Virtual Laboratory [1–3].

The Base Astrophysical Targets

Nowadays, the data in in the field of astrophysics modeling are especially important and needed for simulations/calculations. For example the A + M data for hydrogen are important for development of atmosphere models of solar and near solar type stars and for radiative transport investigations as well as an understanding of the kinetics of stellar and other astrophysical plasmas [4,5]. Modern codes for stellar atmosphere modelling, like e.g., PHOENIX (see e.g., [6–8]) require the knowledge of atomic data, so that the access to such atomic data, via online databases become very important.

The helium A + M data are of interest particularly for helium-rich white dwarf atmospheres investigations [9,10]. Such data are also important in modelling early Universe chemistry (see the paper of Coppola et al., 2013 [11]). The data for H and some metal atoms like Li, Na, Si are important for the exploring of the geo-cosmical plasmas, the interstellar medium as well as for studies of the early Universe chemistry and for the modelling of stellar and solar atmospheres (see, e.g., [12,13]).

Recently, in the papers [14–18] it has been pointed out that the photodissociation of the diatomic molecular ion in the symmetric and non-symmetric cases, are of astrophysical relevance and could be important in modeling of specific stellar atmosphere layers and they should be included in some chemical models. In the symmetric case, it was considered the processes of molecular ion photodissociation (bound-free) and ion-atom photoassociation (free-bound):

$$h\nu + A_2^+ \Longleftrightarrow A + A^+, \tag{1}$$

where A and A^+ are atom and ion in their ground states, and A_2^+ is molecular-ion in the ground electronic state.

In the non-symmetric case, the similar processes of photodissociation/photoassociation are:

$$h\nu + AM^+ \Longleftrightarrow A^+ + M, \tag{2}$$

where M is an atom whose ionization potential is less than the corresponding value for atom A. AM^+ is also molecular-ion in the ground electronic state.

In the general case molecular ion A_2^+ or AM^+ can be in one of the states from the group which contains the ground electronic state. For the solar atmosphere, A usually denotes atom H(1s) and M one of the relevant metal atoms (Mg, Si, Ca, Na) [14–16], but there are cases where A = He, and M = H, Mg, Si, Ca, Na. For the helium-rich white dwarf atmospheres A denotes He($1s^2$) and M denotes, H(1s), and eventually carbon or oxygen [19,20].

Recently, the results from [16] show the importance of including the symmetric processes with A = H(1s) in the stellar atmosphere models like [5]. Also, for modeling the DB white dwarf atmospheres results for case A = He($1s^2$) have been used (Koester 2016, private communication). The photodissociation of HeH^+ has been extensively studied both from a theoretical and experimentalist point of view and inserted in chemical networks describing the formation and destruction of primordial molecules.

It is well known [21] that the chemical composition of the primordial gas consists of electrons and species such as: helium- He, He^+, He^{2+} and HeH^+; hydrogen- H, H^-, H^+, H_2^+ and H_2; deuterium- D, D^+, HD, HD^+ and HD^-; lithium- Li, Li^+, Li^-, LiH^- and LiH^+. Evaluation of chemical abundances in the standard BB model are calculated from a set of chemical reactions for the early universe [21] and is presented at Figure 1 from [21]. One can see that among them are species like molecular ions H_2^+, HD^+, HeH^+, etc., whose role in the primordial star formation is important.

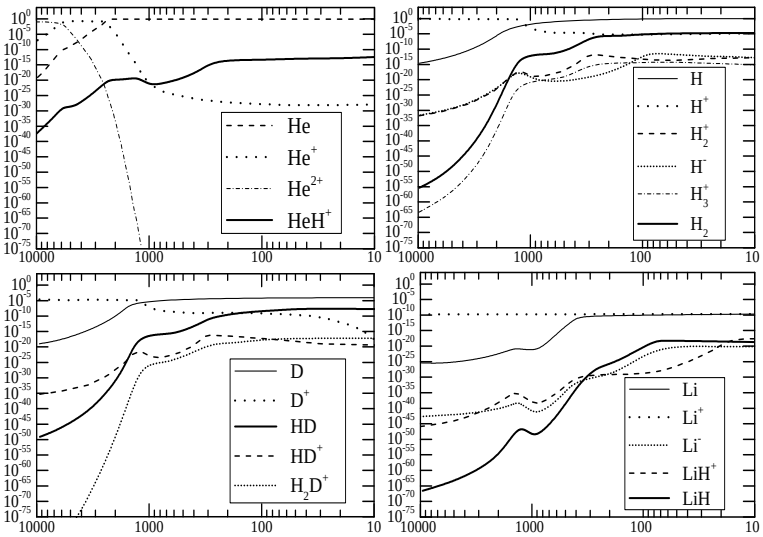

Figure 1. Evaluation of chemical abundances in the standard Big Bang (BB) model. Vertical axes are the relative abundances and the horizontal axes are relative to the redshift (taken from [21]).

2. MolD

2.1. Database Description

MolD database contains cross-sections for photodissociation processes [22], as well as corresponding data on molecular species and molecular state characterisations. MolD project is part of Serbian Virtual Observatory (SerVO)[1] and Virtual Atomic and Molecular Data Center (VAMDC)[2] (see Figure 2).

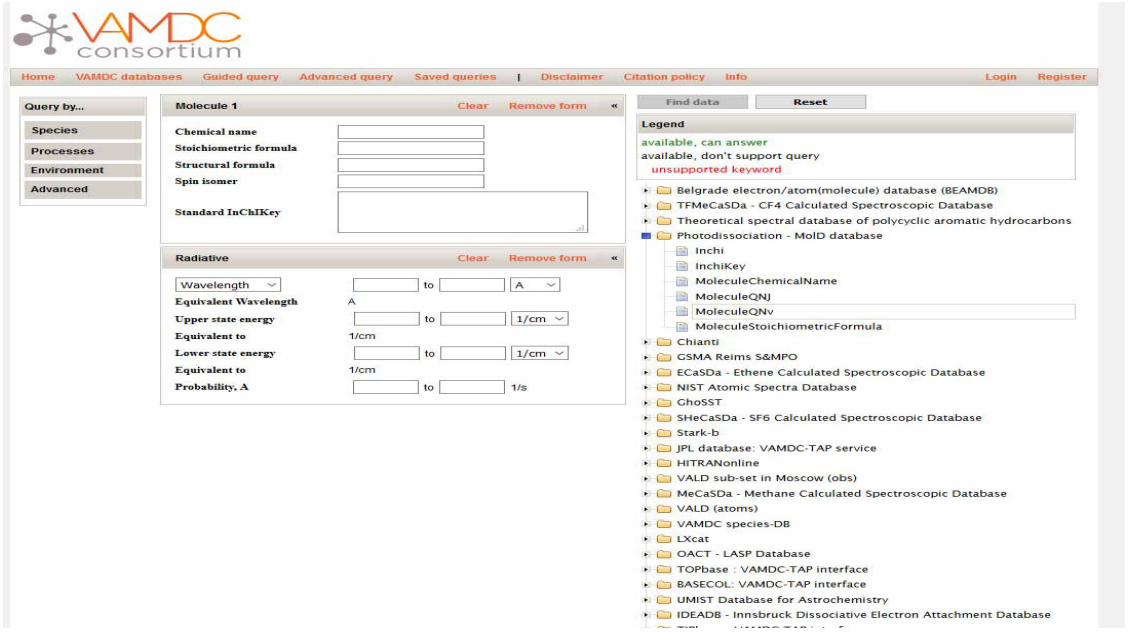

Figure 2. Snapshot from the query page from the Virtual Atomic and Molecular Data Center (VAMDC) portal.

MolD application is implemented as a customisation and extension of NodeSoftware provided by VAMDC. It complies to VAMDC interoperability standards and protocols for distributed remote queries. The underlying technology is Python-based, with Django as a Web framework [23], MySQL as a relational database system [24]. The web application runs on Apache web server.

The data model of MolD application is tailored to specifically suit the needs of the theoretical photodissociation data, and yet to easily map onto VAMDC's standardized XSAMS[3] (XML Schema for Atoms, Molecules and Solids format) schema for representation and exchange of atomic and molecular data[4].

2.2. Accessing MolD Data

MolD data can be accessed in several ways:

- Via MolD homepage (http://servo.aob.rs/mold). There is an AJAX-enabled (Asynchronous JavaScript and XML) web form for data querying as well as calculating and plotting average thermal cross sections along available wavelengths for a given temperatiure.

---

1 http://servo.aob.rs
2 http://vamdc.eu
3 http://vamdc-standards.readthedocs.io/en/latest/dataModel/vamdcxsams/structure.html
4 http://standards.vamdc.eu

- Via VAMDC portal (http://portal.vamdc.eu), where one can pose a distributed query to 30 databases across the European scientific institutes.
- Via standalone applications which support VAMDC-TAP (Table Access Protoco) for data access and tranformation to VAMDC-XSAMS.

During 2017, MolD entered *stage 3* of development. Currently, the database includes cross-section data for processes which involve species such as He_2^+, H_2^+, MgH^+, HeH^+, LiH^+, NaH^+. These processes are important for exploring of the interstellar medium, the early Universe chemistry as well as the modeling of different stellar and solar atmospheres (see papers [11,15,16,20,22]).

Our plans include transition to new versions of Django framework and NodeSoftware, with ongoing incremental inclusion of A + M data from our papers. We also intend to develop a more intuitive interface for querying and presentation of multidimensional data on our website.

2.3. Example: H_2^+ Molecular Ion

MolD is available online from the end of 2014 and it contains the data for the photodissociation processes Equation (1) with $A = \mathrm{H}(1s)$ and $A = \mathrm{He}(1s^2)$. Also it contains the relevant data for some other non-symmetric photodissociation processes Equation (2) where M = Li, Na, Mg or He.

The methods of calculation. The cross-sections for the photodissociation of individual ro-vibrational state of the considered molecular ion H_2^+ is determined in the dipole approximation [14]:

$$\sigma_{J,v}(\lambda) = \frac{8\pi^3}{3\lambda}\left[\frac{(J+1)|D_{E,J+1;v,J}|^2 + J|D_{E,J-1;v,J}|^2}{2J+1}\right], \tag{3}$$

and the corresponding averaged thermal cross sections are given by:

$$\sigma_{\mathrm{phd}}(\lambda, T) = \frac{1}{Z}\sum_J\sum_v g_{J;v}(2J+1)e^{-\frac{E_{Jv}-E_{00}}{k_B T}}\sigma_{J,v}(\lambda). \tag{4}$$

where T is temperature, λ-wavelength, $D_{E,J+1;v,J}$ is the radial matrix element [25], E_{Jv} is the energy of the individual states with the angular and vibrational quantum numbers J and v respectively, and Z is the partition function

$$Z = \sum_J\sum_v g_{J;v}(2J+1)e^{-\frac{E_{Jv}-E_{0,0}}{k_B T}}. \tag{5}$$

In this expression the product $g_{J;v} \times (2J+1)$ is the statistical weight of the considered state and the coefficient $g_{J;v}$ depends on the "the spin of the nuclei".

The photo-dissociation crosssection $\sigma_{phd}(\lambda, T)$ given by Equation (4), as well as the coefficients $K_{ia}(\lambda, T)$, are determined within the approximation where the processes are treated as the result of the radiative transitions between the ground and the first excited adiabatic electronic state of the molecular ion H_2^+ which are caused by the interaction of the electron component of the ion-atom system with the free electromagnetic field taken in the dipole approximation.

For determination of $\sigma_{phd}(\lambda, T)$, as well as the coefficients $K_{ia}(\lambda, T)$ it is important to know the dipole matrix element $D_{12}(R)$ defined by relations

$$D_{12}(R) = \mathbf{D}_{12}(\mathbf{R}), \quad \mathbf{D}_{12}(\mathbf{R}) = \langle 1|\mathbf{D}(\mathbf{R})|2\rangle \tag{6}$$

where $R = |\mathbf{R}|$ and $\mathbf{D}(\mathbf{R})$ is the operator of electron dipole momentum. The mentioned adiabatic electronic states, $X^2\sum_g^+$ and $A^2\sum_u^-$, are denoted here with $|1\rangle$ and $|2\rangle$ and R is the internuclear distance in the considered ion-atom system.

The described mechanism of the processes causes absorption of the photon with energy ϵ_λ near the resonant point $R = R_\lambda$, where R_λ is the root of the equation

$$U_{12}(R) \equiv U_1(R) - U_2(R) = \epsilon_\lambda. \tag{7}$$

where $U_1(R)$ corresponds to the ground electronic state, and $U_2(R)$—to the first excited electronic state.

In Figure 3 are presented the data for $\sigma_{J,v}(\lambda)$ Equation (3) for the case $J = 0$ and $v = 10$, in the wavelength region $50\,\text{nm} \leq \lambda \leq 1500\,\text{nm}$.

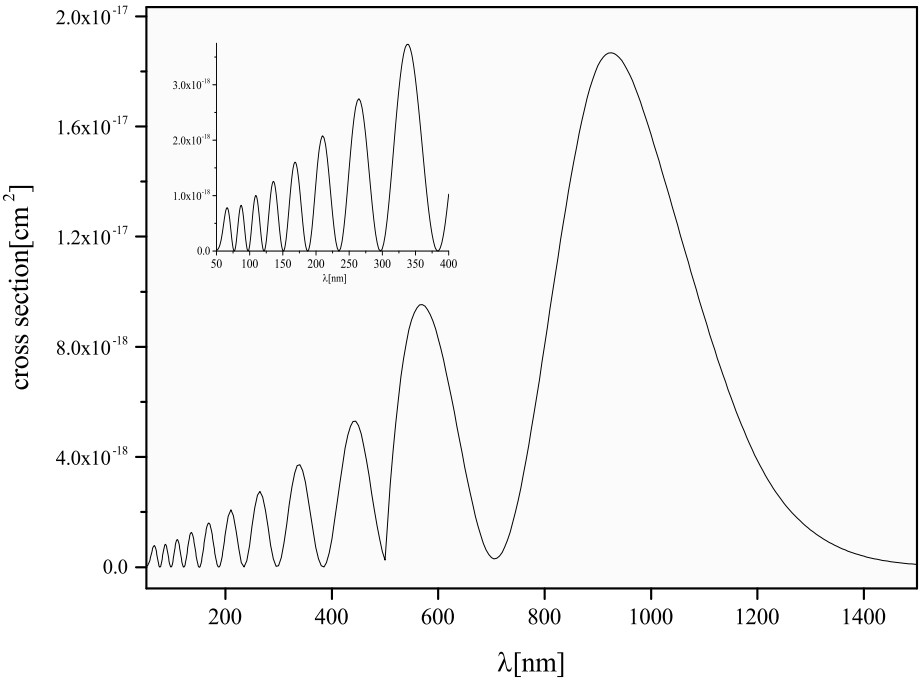

Figure 3. The behaviour of the cross-section $\sigma_{J,v}(\lambda)$ Equation (3) for $J = 0$ and $v = 10$, as a function of λ.

The spectral coefficients. The absorption process (1) i.e., processes of molecular ion photodissociation (bound-free) for the case $A = \text{H}$ is characterized by partial spectral absorption coefficients $\kappa_{ia}(\lambda)$ (see e.g., [25]) taken in the form

$$\kappa_{ia}(\lambda) = \sigma_{phd}(\lambda, T) N(\text{H}_2^+) \tag{8}$$

where $N(\text{H}_2^+)$ is density of the H_2^+ and $\sigma_{phd}(\lambda, T)$ is average cross-section for photo-dissociation of this molecular ion given by Equation (4). As in previous papers [14,25] the partial spectral absorption coefficient $\kappa_{ia}(\lambda)$ is also used in the form

$$\kappa_{ia}(\lambda) = K_{ia}(\lambda, T) N(\text{H}) \text{N}(\text{H}^+) \tag{9}$$

where the coefficient $K_{ia}(\lambda, T)$ is connected with $\sigma_{phd}(\lambda, T)$ by the relations

$$K_{ia}(\lambda, T) = \sigma_{phd}(\lambda, T) \chi^{-1}, \quad \chi = \frac{N(\text{H}) \text{N}(\text{H}^+)}{N(\text{H}_2^+)}. \tag{10}$$

In accordance with the definition of the absorption coefficient $\kappa_{ia}(\lambda)$, the coefficient $K_{ia}(\lambda, T)$ is given in units (cm^5). The results for the average photodissociation cross-section $\sigma_{phd}(\lambda, T)$ for H_2^+ molecular ion are illustrated by Figure 4. The curves in this figure show the behavior of $\sigma_{phd}(\lambda, T)$ as a function of λ for a wide range of temperatures T, which are relevant for the stelar

atmosphere (e.g., solar photosphere). The values of the coefficient $K_{ia}(\lambda, T)$, defined by Equation (10), are presented in the Table 1 for the regions 90 nm $\leq \lambda \leq$ 370 nm with small wavelength steps and for 3000 K $\leq T \leq$ 10,000 K in order to enable easier use (interpolation) of this results. This allows direct calculation of the spectral absorption coefficients during the process of applying a any atmosphere model with the given parameters of plasma and composition.

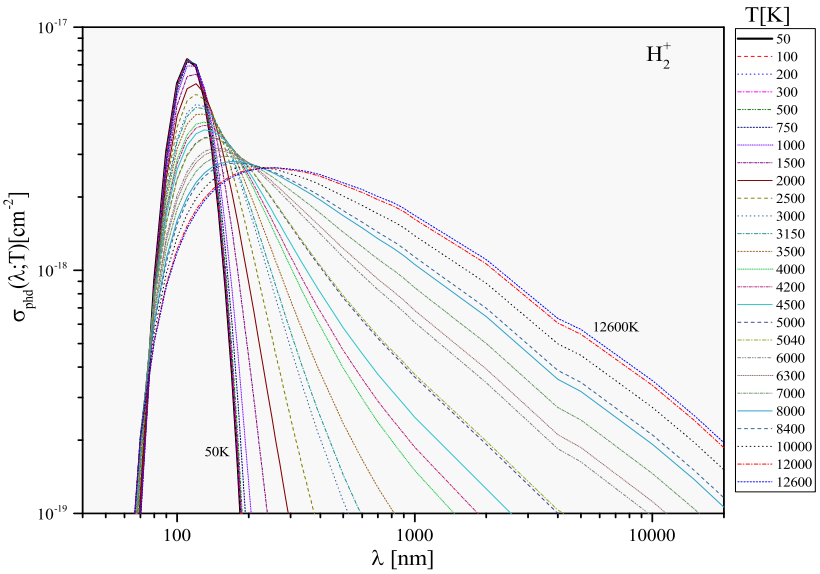

Figure 4. The behaviour of the averaged cross-section $\sigma_{phd}(\lambda, T)$ for photodissociation of the H_2^+ molecular ion, as a function of λ and T.

Table 1. The coefficient $K_{ia}(\mathrm{cm}^5)$ Equation (9) as a function of λ and T.

λ (nm)	3000 K	4000 K	5000 K	6000 K	7000 K	8000 K	9000 K	10,000 K
90	3.50E−37	2.62E−38	5.50E−39	1.93E−39	9.04E−40	5.07E−40	3.20E−40	2.20E−40
91	3.75E−37	2.78E−38	5.80E−39	2.03E−39	9.47E−40	5.30E−40	3.34E−40	2.29E−40
92	3.99E−37	2.94E−38	6.10E−39	2.12E−39	9.90E−40	5.53E−40	3.48E−40	2.39E−40
93	4.23E−37	3.10E−38	6.40E−39	2.22E−39	1.03E−39	5.76E−40	3.62E−40	2.48E−40
94	4.47E−37	3.25E−38	6.69E−39	2.31E−39	1.07E−39	5.98E−40	3.76E−40	2.57E−40
95	4.71E−37	3.41E−38	6.98E−39	2.41E−39	1.12E−39	6.20E−40	3.89E−40	2.66E−40
96	4.95E−37	3.56E−38	7.27E−39	2.50E−39	1.16E−39	6.42E−40	4.03E−40	2.75E−40
97	5.18E−37	3.70E−38	7.54E−39	2.59E−39	1.20E−39	6.63E−40	4.16E−40	2.84E−40
98	5.40E−37	3.85E−38	7.82E−39	2.68E−39	1.24E−39	6.85E−40	4.29E−40	2.92E−40
99	5.62E−37	3.99E−38	8.08E−39	2.76E−39	1.27E−39	7.05E−40	4.41E−40	3.01E−40
100	5.82E−37	4.12E−38	8.34E−39	2.85E−39	1.31E−39	7.26E−40	4.54E−40	3.09E−40
101	6.03E−37	4.25E−38	8.59E−39	2.93E−39	1.35E−39	7.46E−40	4.66E−40	3.17E−40
102	6.22E−37	4.38E−38	8.83E−39	3.01E−39	1.38E−39	7.65E−40	4.78E−40	3.26E−40
103	6.40E−37	4.50E−38	9.06E−39	3.09E−39	1.42E−39	7.84E−40	4.90E−40	3.34E−40
104	6.58E−37	4.62E−38	9.29E−39	3.16E−39	1.45E−39	8.03E−40	5.02E−40	3.41E−40
105	6.74E−37	4.73E−38	9.51E−39	3.24E−39	1.49E−39	8.21E−40	5.13E−40	3.49E−40
106	6.90E−37	4.83E−38	9.72E−39	3.31E−39	1.52E−39	8.39E−40	5.24E−40	3.57E−40
107	7.04E−37	4.93E−38	9.92E−39	3.38E−39	1.55E−39	8.57E−40	5.35E−40	3.64E−40
108	7.18E−37	5.03E−38	1.01E−38	3.44E−39	1.58E−39	8.74E−40	5.46E−40	3.72E−40
109	7.30E−37	5.11E−38	1.03E−38	3.51E−39	1.61E−39	8.90E−40	5.56E−40	3.79E−40
110	7.41E−37	5.20E−38	1.05E−38	3.57E−39	1.64E−39	9.06E−40	5.67E−40	3.86E−40
111	7.52E−37	5.28E−38	1.06E−38	3.62E−39	1.67E−39	9.22E−40	5.77E−40	3.93E−40
112	7.61E−37	5.35E−38	1.08E−38	3.68E−39	1.69E−39	9.37E−40	5.86E−40	3.99E−40
113	7.69E−37	5.42E−38	1.09E−38	3.73E−39	1.72E−39	9.52E−40	5.96E−40	4.06E−40
114	7.77E−37	5.48E−38	1.11E−38	3.79E−39	1.74E−39	9.66E−40	6.05E−40	4.12E−40
115	7.83E−37	5.54E−38	1.12E−38	3.83E−39	1.77E−39	9.80E−40	6.14E−40	4.18E−40
116	7.89E−37	5.59E−38	1.13E−38	3.88E−39	1.79E−39	9.93E−40	6.22E−40	4.24E−40

Table 1. *Cont.*

λ (nm)	3000 K	4000 K	5000 K	6000 K	7000 K	8000 K	9000 K	10,000 K
117	7.93E−37	5.63E−38	1.15E−38	3.93E−39	1.81E−39	1.01E−39	6.31E−40	4.30E−40
118	7.97E−37	5.68E−38	1.16E−38	3.97E−39	1.83E−39	1.02E−39	6.39E−40	4.36E−40
119	8.00E−37	5.71E−38	1.17E−38	4.01E−39	1.85E−39	1.03E−39	6.46E−40	4.42E−40
120	8.02E−37	5.75E−38	1.18E−38	4.05E−39	1.87E−39	1.04E−39	6.54E−40	4.47E−40
121	8.03E−37	5.78E−38	1.18E−38	4.08E−39	1.89E−39	1.05E−39	6.62E−40	4.52E−40
122	8.04E−37	5.80E−38	1.19E−38	4.12E−39	1.91E−39	1.06E−39	6.69E−40	4.57E−40
123	8.04E−37	5.82E−38	1.20E−38	4.15E−39	1.93E−39	1.07E−39	6.76E−40	4.62E−40
124	8.03E−37	5.84E−38	1.21E−38	4.18E−39	1.94E−39	1.08E−39	6.83E−40	4.67E−40
125	8.01E−37	5.85E−38	1.21E−38	4.21E−39	1.96E−39	1.09E−39	6.89E−40	4.72E−40
126	7.99E−37	5.86E−38	1.22E−38	4.23E−39	1.97E−39	1.10E−39	6.96E−40	4.77E−40
127	7.97E−37	5.87E−38	1.22E−38	4.26E−39	1.99E−39	1.11E−39	7.02E−40	4.81E−40
128	7.94E−37	5.87E−38	1.23E−38	4.28E−39	2.00E−39	1.12E−39	7.08E−40	4.86E−40
129	7.90E−37	5.87E−38	1.23E−38	4.30E−39	2.01E−39	1.13E−39	7.14E−40	4.90E−40
130	7.86E−37	5.87E−38	1.23E−38	4.32E−39	2.03E−39	1.14E−39	7.19E−40	4.94E−40
131	7.81E−37	5.86E−38	1.24E−38	4.34E−39	2.04E−39	1.15E−39	7.25E−40	4.98E−40
132	7.76E−37	5.86E−38	1.24E−38	4.36E−39	2.05E−39	1.15E−39	7.30E−40	5.02E−40
133	7.70E−37	5.84E−38	1.24E−38	4.37E−39	2.06E−39	1.16E−39	7.35E−40	5.06E−40
134	7.65E−37	5.83E−38	1.24E−38	4.39E−39	2.07E−39	1.17E−39	7.40E−40	5.10E−40
135	7.58E−37	5.82E−38	1.24E−38	4.40E−39	2.08E−39	1.17E−39	7.45E−40	5.13E−40
136	7.52E−37	5.80E−38	1.24E−38	4.41E−39	2.09E−39	1.18E−39	7.49E−40	5.17E−40
137	7.45E−37	5.78E−38	1.24E−38	4.42E−39	2.09E−39	1.19E−39	7.54E−40	5.20E−40
138	7.38E−37	5.76E−38	1.24E−38	4.43E−39	2.10E−39	1.19E−39	7.58E−40	5.24E−40
139	7.31E−37	5.73E−38	1.24E−38	4.43E−39	2.11E−39	1.20E−39	7.62E−40	5.27E−40
140	7.24E−37	5.71E−38	1.24E−38	4.44E−39	2.12E−39	1.20E−39	7.66E−40	5.30E−40
141	7.16E−37	5.68E−38	1.24E−38	4.45E−39	2.12E−39	1.21E−39	7.70E−40	5.33E−40
142	7.08E−37	5.65E−38	1.24E−38	4.45E−39	2.13E−39	1.21E−39	7.74E−40	5.36E−40
143	7.00E−37	5.62E−38	1.23E−38	4.45E−39	2.13E−39	1.22E−39	7.77E−40	5.39E−40
144	6.92E−37	5.59E−38	1.23E−38	4.46E−39	2.14E−39	1.22E−39	7.80E−40	5.41E−40
145	6.84E−37	5.56E−38	1.23E−38	4.46E−39	2.14E−39	1.22E−39	7.84E−40	5.44E−40
146	6.76E−37	5.52E−38	1.23E−38	4.46E−39	2.15E−39	1.23E−39	7.87E−40	5.46E−40
147	6.68E−37	5.49E−38	1.22E−38	4.46E−39	2.15E−39	1.23E−39	7.90E−40	5.49E−40
148	6.59E−37	5.45E−38	1.22E−38	4.46E−39	2.15E−39	1.23E−39	7.93E−40	5.51E−40
149	6.51E−37	5.42E−38	1.22E−38	4.45E−39	2.15E−39	1.24E−39	7.95E−40	5.54E−40
150	6.42E−37	5.38E−38	1.21E−38	4.45E−39	2.16E−39	1.24E−39	7.98E−40	5.56E−40
151	6.34E−37	5.34E−38	1.21E−38	4.45E−39	2.16E−39	1.24E−39	8.01E−40	5.58E−40
152	6.25E−37	5.30E−38	1.20E−38	4.44E−39	2.16E−39	1.25E−39	8.03E−40	5.60E−40
153	6.17E−37	5.26E−38	1.20E−38	4.44E−39	2.16E−39	1.25E−39	8.05E−40	5.62E−40
154	6.08E−37	5.22E−38	1.20E−38	4.43E−39	2.16E−39	1.25E−39	8.08E−40	5.64E−40
155	6.00E−37	5.18E−38	1.19E−38	4.43E−39	2.16E−39	1.25E−39	8.10E−40	5.66E−40
156	5.91E−37	5.14E−38	1.19E−38	4.42E−39	2.17E−39	1.25E−39	8.12E−40	5.68E−40
157	5.83E−37	5.10E−38	1.18E−38	4.42E−39	2.17E−39	1.26E−39	8.14E−40	5.70E−40
158	5.74E−37	5.06E−38	1.18E−38	4.41E−39	2.17E−39	1.26E−39	8.16E−40	5.72E−40
159	5.66E−37	5.02E−38	1.17E−38	4.40E−39	2.17E−39	1.26E−39	8.18E−40	5.73E−40
160	5.58E−37	4.98E−38	1.17E−38	4.39E−39	2.17E−39	1.26E−39	8.19E−40	5.75E−40
162	5.41E−37	4.90E−38	1.16E−38	4.37E−39	2.16E−39	1.26E−39	8.22E−40	5.78E−40
163	5.33E−37	4.85E−38	1.15E−38	4.36E−39	2.16E−39	1.26E−39	8.24E−40	5.79E−40
164	5.25E−37	4.81E−38	1.14E−38	4.35E−39	2.16E−39	1.27E−39	8.25E−40	5.81E−40
165	5.17E−37	4.77E−38	1.14E−38	4.34E−39	2.16E−39	1.27E−39	8.27E−40	5.82E−40
166	5.09E−37	4.73E−38	1.13E−38	4.33E−39	2.16E−39	1.27E−39	8.28E−40	5.83E−40
167	5.02E−37	4.68E−38	1.13E−38	4.32E−39	2.16E−39	1.27E−39	8.29E−40	5.85E−40
168	4.94E−37	4.64E−38	1.12E−38	4.31E−39	2.16E−39	1.27E−39	8.30E−40	5.86E−40
169	4.86E−37	4.60E−38	1.12E−38	4.30E−39	2.15E−39	1.27E−39	8.31E−40	5.87E−40
170	4.79E−37	4.56E−38	1.11E−38	4.29E−39	2.15E−39	1.27E−39	8.32E−40	5.88E−40
171	4.71E−37	4.52E−38	1.10E−38	4.27E−39	2.15E−39	1.27E−39	8.33E−40	5.89E−40
172	4.64E−37	4.48E−38	1.10E−38	4.26E−39	2.15E−39	1.27E−39	8.34E−40	5.90E−40
173	4.57E−37	4.43E−38	1.09E−38	4.25E−39	2.14E−39	1.27E−39	8.34E−40	5.91E−40
174	4.50E−37	4.39E−38	1.09E−38	4.24E−39	2.14E−39	1.27E−39	8.35E−40	5.92E−40
175	4.43E−37	4.35E−38	1.08E−38	4.22E−39	2.14E−39	1.27E−39	8.36E−40	5.93E−40

Table 1. *Cont.*

λ (nm)	3000 K	4000 K	5000 K	6000 K	7000 K	8000 K	9000 K	10,000 K
176	4.36E−37	4.31E−38	1.07E−38	4.21E−39	2.13E−39	1.27E−39	8.36E−40	5.94E−40
177	4.29E−37	4.27E−38	1.07E−38	4.20E−39	2.13E−39	1.27E−39	8.37E−40	5.94E−40
178	4.22E−37	4.23E−38	1.06E−38	4.18E−39	2.13E−39	1.27E−39	8.37E−40	5.95E−40
179	4.15E−37	4.19E−38	1.06E−38	4.17E−39	2.12E−39	1.27E−39	8.38E−40	5.96E−40
180	4.09E−37	4.15E−38	1.05E−38	4.16E−39	2.12E−39	1.27E−39	8.38E−40	5.96E−40
181	4.02E−37	4.11E−38	1.04E−38	4.14E−39	2.12E−39	1.27E−39	8.38E−40	5.97E−40
182	3.96E−37	4.07E−38	1.04E−38	4.13E−39	2.11E−39	1.26E−39	8.39E−40	5.98E−40
183	3.90E−37	4.03E−38	1.03E−38	4.11E−39	2.11E−39	1.26E−39	8.39E−40	5.98E−40
184	3.84E−37	4.00E−38	1.03E−38	4.10E−39	2.11E−39	1.26E−39	8.39E−40	5.99E−40
185	3.78E−37	3.96E−38	1.02E−38	4.09E−39	2.10E−39	1.26E−39	8.39E−40	5.99E−40
186	3.72E−37	3.92E−38	1.01E−38	4.07E−39	2.10E−39	1.26E−39	8.39E−40	6.00E−40
187	3.66E−37	3.88E−38	1.01E−38	4.06E−39	2.09E−39	1.26E−39	8.39E−40	6.00E−40
188	3.60E−37	3.84E−38	1.00E−38	4.04E−39	2.09E−39	1.26E−39	8.40E−40	6.01E−40
189	3.54E−37	3.81E−38	9.95E−39	4.03E−39	2.09E−39	1.26E−39	8.40E−40	6.01E−40
190	3.49E−37	3.77E−38	9.89E−39	4.01E−39	2.08E−39	1.26E−39	8.40E−40	6.02E−40
191	3.43E−37	3.73E−38	9.83E−39	4.00E−39	2.08E−39	1.26E−39	8.39E−40	6.02E−40
192	3.38E−37	3.70E−38	9.77E−39	3.98E−39	2.07E−39	1.26E−39	8.39E−40	6.02E−40
193	3.33E−37	3.66E−38	9.71E−39	3.97E−39	2.07E−39	1.25E−39	8.39E−40	6.03E−40
194	3.27E−37	3.63E−38	9.65E−39	3.95E−39	2.06E−39	1.25E−39	8.39E−40	6.03E−40
195	3.22E−37	3.59E−38	9.59E−39	3.94E−39	2.06E−39	1.25E−39	8.39E−40	6.03E−40
196	3.17E−37	3.56E−38	9.54E−39	3.92E−39	2.06E−39	1.25E−39	8.39E−40	6.03E−40
197	3.12E−37	3.52E−38	9.48E−39	3.91E−39	2.05E−39	1.25E−39	8.38E−40	6.04E−40
198	3.08E−37	3.49E−38	9.42E−39	3.89E−39	2.05E−39	1.25E−39	8.38E−40	6.04E−40
199	3.03E−37	3.46E−38	9.36E−39	3.88E−39	2.04E−39	1.25E−39	8.38E−40	6.04E−40
200	2.98E−37	3.42E−38	9.31E−39	3.86E−39	2.04E−39	1.24E−39	8.38E−40	6.04E−40
205	2.76E−37	3.26E−38	9.03E−39	3.79E−39	2.01E−39	1.24E−39	8.35E−40	6.04E−40
210	2.56E−37	3.11E−38	8.75E−39	3.71E−39	1.99E−39	1.23E−39	8.33E−40	6.04E−40
215	2.37E−37	2.97E−38	8.49E−39	3.64E−39	1.96E−39	1.22E−39	8.29E−40	6.03E−40
220	2.20E−37	2.83E−38	8.24E−39	3.57E−39	1.94E−39	1.21E−39	8.25E−40	6.02E−40
225	2.04E−37	2.71E−38	7.99E−39	3.50E−39	1.91E−39	1.20E−39	8.21E−40	6.01E−40
230	1.90E−37	2.59E−38	7.76E−39	3.43E−39	1.89E−39	1.19E−39	8.17E−40	5.99E−40
235	1.77E−37	2.48E−38	7.53E−39	3.36E−39	1.86E−39	1.18E−39	8.13E−40	5.98E−40
240	1.66E−37	2.37E−38	7.32E−39	3.30E−39	1.84E−39	1.17E−39	8.08E−40	5.96E−40
245	1.55E−37	2.27E−38	7.11E−39	3.23E−39	1.81E−39	1.16E−39	8.04E−40	5.94E−40
250	1.45E−37	2.18E−38	6.92E−39	3.17E−39	1.79E−39	1.15E−39	7.99E−40	5.92E−40
255	1.36E−37	2.09E−38	6.73E−39	3.11E−39	1.76E−39	1.13E−39	7.94E−40	5.90E−40
260	1.27E−37	2.01E−38	6.54E−39	3.05E−39	1.74E−39	1.12E−39	7.89E−40	5.87E−40
265	1.20E−37	1.93E−38	6.37E−39	2.99E−39	1.72E−39	1.11E−39	7.83E−40	5.84E−40
270	1.12E−37	1.85E−38	6.20E−39	2.94E−39	1.69E−39	1.10E−39	7.78E−40	5.82E−40
275	1.06E−37	1.78E−38	6.04E−39	2.89E−39	1.67E−39	1.09E−39	7.72E−40	5.79E−40
280	9.99E−38	1.72E−38	5.89E−39	2.83E−39	1.65E−39	1.08E−39	7.67E−40	5.76E−40
285	9.43E−38	1.66E−38	5.74E−39	2.78E−39	1.63E−39	1.07E−39	7.62E−40	5.73E−40
290	8.92E−38	1.60E−38	5.60E−39	2.73E−39	1.61E−39	1.06E−39	7.56E−40	5.70E−40
295	8.45E−38	1.54E−38	5.47E−39	2.69E−39	1.59E−39	1.05E−39	7.51E−40	5.67E−40
300	8.00E−38	1.49E−38	5.34E−39	2.64E−39	1.57E−39	1.04E−39	7.46E−40	5.64E−40
305	7.60E−38	1.44E−38	5.22E−39	2.60E−39	1.55E−39	1.03E−39	7.41E−40	5.61E−40
310	7.22E−38	1.39E−38	5.10E−39	2.56E−39	1.53E−39	1.02E−39	7.36E−40	5.59E−40
315	6.86E−38	1.35E−38	4.99E−39	2.52E−39	1.51E−39	1.01E−39	7.32E−40	5.56E−40
320	6.53E−38	1.31E−38	4.88E−39	2.48E−39	1.49E−39	1.01E−39	7.27E−40	5.53E−40
325	6.23E−38	1.27E−38	4.78E−39	2.44E−39	1.48E−39	9.96E−40	7.22E−40	5.51E−40
330	5.94E−38	1.23E−38	4.68E−39	2.40E−39	1.46E−39	9.88E−40	7.17E−40	5.48E−40
335	5.67E−38	1.19E−38	4.58E−39	2.37E−39	1.44E−39	9.79E−40	7.13E−40	5.45E−40
340	5.42E−38	1.16E−38	4.49E−39	2.33E−39	1.43E−39	9.71E−40	7.08E−40	5.43E−40
345	5.19E−38	1.13E−38	4.40E−39	2.30E−39	1.41E−39	9.63E−40	7.04E−40	5.40E−40

Table 1. *Cont.*

λ (nm)	3000 K	4000 K	5000 K	6000 K	7000 K	8000 K	9000 K	10,000 K
350	4.97E−38	1.09E−38	4.31E−39	2.26E−39	1.40E−39	9.55E−40	6.99E−40	5.37E−40
355	4.76E−38	1.06E−38	4.23E−39	2.23E−39	1.38E−39	9.47E−40	6.95E−40	5.35E−40
360	4.57E−38	1.04E−38	4.15E−39	2.20E−39	1.37E−39	9.39E−40	6.90E−40	5.32E−40
365	4.38E−38	1.01E−38	4.07E−39	2.17E−39	1.35E−39	9.32E−40	6.86E−40	5.29E−40
370	4.21E−38	9.82E−39	4.00E−39	2.14E−39	1.34E−39	9.24E−40	6.81E−40	5.26E−40

Solar atmosphere: absorption processes. The influence of radiation processes (1) can bee estimated by comparing their intensities with the intensities of known concurrent radiation processes, namely:

$$\varepsilon_\lambda + \begin{cases} \mathrm{H}^- \\ \mathrm{H} + e' \end{cases} \Rightarrow \mathrm{H} + e'' \tag{11}$$

$$\varepsilon_\lambda + \begin{cases} \mathrm{H}^* \\ \mathrm{H}^+ + e' \end{cases} \Rightarrow \mathrm{H}^+ + e'' \tag{12}$$

The relative contributions of the processes (1), with respect to processes (11) and (12), is described by the quantities F_κ defined by relation

$$F_\kappa = \frac{\kappa_{ia}}{\kappa_{ea} + \kappa_{ei}} \tag{13}$$

where κ_{ea} is absorption spectral coefficient of processes (11) and κ_{ei} is absorption spectral coefficient of processes (12) (see papers [14,16]).

Similarly to the He case in DB white dwarf atmosphere [25] calculations of the absorption coefficient were performed for the solar photosphere and lower chromosphere by means of a standard Solar atmosphere model [5], and the total contribution of the processes (1) to the solar opacity was estimated [16]. The results of the calculations of the parameter F_κ for 92 nm $\leq \lambda \leq$ 350 nm are presented in Figure 5. The figure show that in the significant part of the considered region of altitudes (-75 km $\leq h \leq$ 1065 km) the absorption process (1) together give the contribution which varies from about 10% to about 90% of the contribution of the absorption process (11) and (12), which are considered as the main absorption processes [16].

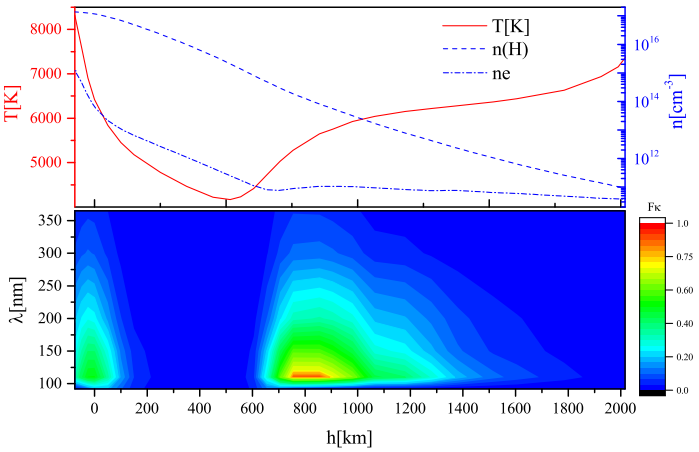

Figure 5. Upper panel: The behavior of the temperature T, N_H and Ne as a function of height h within the considered part of the solar atmosphere model; lower panel: A surface plot of the quantity $F_\kappa = \kappa_{ia}/(\kappa_{ea} + \kappa_{ei})$ (data taken from [14]) as a function of λ and height h for a model of the solar photosphere [5].

On the basis of the above, it can be concluded that photodissociation processes represent important channels for destruction of molecules in lot of astrophysical environments and features of the interacting radiation are important in their spectral analyses.

3. Future Developments and Concluding Remarks

Exploitation the full potential of A + M data and database services is an ongoing challenge in virtual data centers. There are still many limitations and problems that users are facing with such as poor documentation, missing of data evaluation, no open access, etc. The aim of MolD database is to be accessible, and be used by the wider scientific community, through VAMDC and to follow certain protocols and defined rules in order to eliminate such limitations and problems.

The next step of development i.e., the stage three of MolD development will be the implementation of possibility to fit the tabulated data. We plan to develop fitting formulas for photodissociation cross section as the function of the temperature and wavelength. Also, we intend to update the current database with newly calculated/measured data.

The continuation of such developments and services such as constantly updated online A + M database, is crucial in the field of astrophysics and modern physics due to its rapid development and make an immense impact on the way science is done in the developing world.

Acknowledgments: The authors are thankful to the Ministry of Education, Science and Technological Development of the Republic of Serbia for the support of this work within the projects 176002 and III44002. This work has also been supported by the VAMDC (Virtual Atomic and Molecular Data Centre). VAMDC is funded under the Combination of Collaborative Projects and Coordination and Support Actions Funding Scheme of The Seventh Framework Program. We acknowledge the contribution of late A.A. Mihajlov who collected and calculated much of the data that are presented within the MolD database.

Author Contributions: This work is based on the numerous contributions of all the authors.

Conflicts of Interest: The authors declare no conflict of interest.

References

1. Marinković, B.P.; Vujčić, V.; Sushko, G.; Vudragović, D.; Marinković, D.B.; Đorđević, S.; Ivanović, S.; Nešić, M.; Jevremović, D.; Solov'yov, A.V.; et al. Development of collisional data base for elementary processes of electron scattering by atoms and molecules. *Nucl. Instr. Meth. Phys. Res. B* **2015**, *354*, 90–95.
2. Dubernet, M.L.; Antony, B.; Ba, Y.A.; Babikov, Y.L.; Bartschat, K.; Boudon, V.; Braams, B.; Chung, H.K.; Daniel, F.; Delahaye, F.; et al. The virtual atomic and molecular data centre (VAMDC) consortium. *J. Phys. B* **2016**, *49*, 074003.
3. Marinković, B.P.; Jevremović, D.; Srećković, V.A.; Vujčić, V.; Ignjatović, L.M.; Dimitrijević, M.S.; Mason, N.J. BEAMDB and MolD—Databases for atomic and molecular collisional and radiative processes: Belgrade nodes of VAMDC. *Eur. Phys. J. D* **2017**, *71*, 158.
4. Christensen-Dalsgaard, J.; Dappen, W.; Ajukov, S.; Anderson, E.; Antia, H.; Basu, S.; Baturin, V.; Berthomieu, G.; Chaboyer, B.; Chitre, S.; et al. The current state of solar modeling. *Science* **1996**, *272*, 1286.
5. Fontenla, J.; Curdt, W.; Haberreiter, M.; Harder, J.; Tian, H. Semiempirical models of the solar atmosphere. III. Set of non-LTE models for far-ultraviolet/extreme-ultraviolet irradiance computation. *Astrophys. J.* **2009**, *707*, 482.
6. Hauschildt, P.; Baron, E. Cool stellar atmospheres with PHOENIX. *Mem. Soc. Astron. Ital. Suppl.* **2005**, *7*, 140.
7. Hauschildt, P.H.; Baron, E. A 3D radiative transfer framework-VI. PHOENIX/3D example applications. *Astron. Astrophys.* **2010**, *509*, A36.
8. Husser, T.O.; Wende-von Berg, S.; Dreizler, S.; Homeier, D.; Reiners, A.; Barman, T.; Hauschildt, P.H. A new extensive library of PHOENIX stellar atmospheres and synthetic spectra. *Astron. Astrophys.* **2013**, *553*, A6.
9. Augustovičová, L.; Špirko, V.; Kraemer, W.; Soldán, P. Radiative association of He_2^+ revisited. *Astron. Astrophys.* **2013**, *553*, A42.
10. Koester, D. Model atmospheres for DB white dwarfs. *Astron. Astrophys. Suppl. Ser.* **1980**, *39*, 401–409.
11. Coppola, C.M.; Galli, D.; Palla, F.; Longo, S.; Chluba, J. Non-thermal photons and H_2 formation in the early Universe. *Mon. Not. R. Astron. Soc.* **2013**, *434*, 114–122.

12. Klyucharev, A.; Bezuglov, N.; Matveev, A.; Mihajlov, A.; Ignjatović, L.M.; Dimitrijević, M. Rate coefficients for the chemi-ionization processes in sodium-and other alkali-metal geocosmical plasmas. *New Astron. Rev.* **2007**, *51*, 547–562.
13. Sugimura, K.; Coppola, C.M.; Omukai, K.; Galli, D.; Palla, F. Role of the channel in the primordial star formation under strong radiation field and the critical intensity for the supermassive star formation. *Mon. Not. R. Astron. Soc.* **2015**, *456*, 270–277.
14. Mihajlov, A.; Ignjatovic, L.M.; Sakan, N.; Dimitrijevic, M. The influence of H_2^+-photo-dissociation and ($H + H^+$)-radiative collisions on the solar atmosphere opacity in UV and VUV regions. *Astron. Astrophys.* **2007**, *469*, 749–754.
15. Ignjatović, L.M.; Mihajlov, A.; Srećković, V.; Dimitrijević, M. Absorption non-symmetric ion-atom processes in helium-rich white dwarf atmospheres. *Mon. Not. R. Astron. Soc.* **2014**, *439*, 2342–2350.
16. Srećković, V.; Mihajlov, A.; Ignjatović, L.M.; Dimitrijević, M. Ion-atom radiative processes in the solar atmosphere: Quiet Sun and sunspots. *Adv. Space Res.* **2014**, *54*, 1264–1271.
17. Babb, J.F. State resolved data for radiative association of H and H^+ and for Photodissociation of H_2^+. *Astrophys. J. Suppl. Ser.* **2015**, *216*, 21.
18. Heays, A.; Bosman, A.; van Dishoeck, E. Photodissociation and photoionisation of atoms and molecules of astrophysical interest. *Astron. Astrophys.* **2017**, *602*, A105.
19. Mihajlov, A.; Ignjatović, L.M.; Srećković, V.; Dimitrijević, M.; Metropoulos, A. The non-symmetric ion-atom radiative processes in the stellar atmospheres. *Mon. Not. R. Astron. Soc.* **2013**, *431*, 589–599.
20. Ignjatović, L.M.; Mihajlov, A.; Srećković, V.; Dimitrijević, M. The ion-atom absorption processes as one of the factors of the influence on the sunspot opacity. *Mon. Not. R. Astron. Soc.* **2014**, *441*, 1504–1512.
21. Puy, D.; Dubrovich, V.; Lipovka, A.; Talbi, D.; Vonlanthen, P. Molecular fluorine chemistry in the early Universe. *Astron. Astrophys.* **2007**, *476*, 685–689.
22. Vujčič, V.; Jevremović, D.; Mihajlov, A.; Ignjatović, L.M.; Srećković, V.; Dimitrijević, M.; Malović, M. MOL-D: A Collisional Database and Web Service within the Virtual Atomic and Molecular Data Center. *J. Astrophys. Astron.* **2015**, *36*, 693–703.
23. Forcier, J.; Bissex, P.; Chun, W.J. *Python Web Development with Django*; Addison-Wesley Professional: Indianapolis, IN, USA, 2008.
24. Widenius, M.; Axmark, D. *MySQL Reference Manual: Documentation from the Source*; O'Reilly Media, Inc.: Sebastopol, CA, USA, 2002.
25. Ignjatović, L.M.; Mihajlov, A.; Sakan, N.; Dimitrijević, M.; Metropoulos, A. The total and relative contribution of the relevant absorption processes to the opacity of DB white dwarf atmospheres in the UV and VUV regions. *Mon. Not. R. Astron. Soc.* **2009**, *396*, 2201–2210.